Appendix

A Capacity Analysis

In below we give a formal analysis of the higher capacity of STDCF than rank-1 decomposition.

For simplicity, we assume $C_{in} = C_{out} = 1$, and only consider the linear convolution operator (omitting the addition of bias and non-linear activation).

We derive the spatiotemporal convolution in continuous integral over space and time. The regular spatiotemporal joint convolution is denoted as $I \circledast W(u,t) := \int \int I(u+u', t+t')W(u',t')du'dt'$, with a filter $W(u,t)$, where $u \in \mathbb{R}^2$, and $t \in \mathbb{R}$. Then, the joint convolution generally can be written as

$$J(\lambda) = \sum_{\lambda'} I(\lambda') \circledast W_{(\lambda,\lambda')}$$

where $W_{(\lambda,\lambda')} : \mathbb{R}^2 \times \mathbb{R} \to \mathbb{R}$ is local both in space and in time. The proposed convolution by atom is equivalently to writing $W_{\lambda,\lambda'}$ as

$$W_{(\lambda,\lambda')} = \sum_{i,j} \alpha^{i,j}_{(\lambda,\lambda')} \psi_i(u)\phi_j(t), \quad \alpha^{i,j}_{(\lambda,\lambda')} \in \mathbb{R}, \tag{1}$$

and $a^{(c,c')}_{k,l}$ are freely trainable, and then

$$J(\lambda) = \sum_{\lambda'} \sum_{i,j} \alpha^{i,j}_{(\lambda,\lambda')} I(\lambda') \circledast (\psi_i \otimes \phi_j), \tag{2}$$

where $\psi \otimes \phi$ denotes the tensor-ed atom, namely $\psi \otimes \phi(u,t) = \psi(u)\phi(t)$. For each fixed pair of (λ, λ'), $\{\alpha^{i,j}_{(\lambda,\lambda')}\}_{i,j}$ is a M-by-N matrix, and generally is full rank.

We compare with applying the space convolution and then the temporal convolution sequentially, i.e. the rank-1 3D filter decomposition. In this decomposition, spatial filters are $W_s = W^{(\lambda'',\lambda')}(u)$, temporal filters are $W_t = W^{(\lambda,\lambda'')}(t)$, $\lambda'' \in [C'']$. Then,

$$Z_{\lambda''} = \sum_{\lambda'} X_{\lambda'} *_u W_s^{(\lambda'',\lambda')}, \quad Y_\lambda = \sum_{\lambda''} Z_{\lambda''} *_t W_t^{(\lambda,\lambda'')}, \tag{3}$$

where $*_u, *_t$ denote spatial and temporal convolution. Write $W_s^{(\lambda'',\lambda')}$ and $W_t^{(\lambda,\lambda'')}$ as combination of atoms ψ_i and ϕ_j respectively,

$$W_s^{(\lambda'',\lambda')} = \sum_i m^i_{(\lambda'',\lambda')} \psi_i, \quad W_t^{(\lambda,\lambda'')} = \sum_j n^j_{(\lambda,\lambda'')} \phi_j,$$

then Y_c can also be expressed as (2) where

$$\boldsymbol{\alpha}^{i,j}_{(\lambda,\lambda')} = \sum_{\lambda''=1}^{C''} m^i_{(\lambda'',\lambda')} n^j_{(\lambda,\lambda'')}, \quad i \in [K_u],\, j \in [K_t].$$

Tracking the degree of freedom reveals that $\boldsymbol{\alpha}^{i,j}_{(\lambda,\lambda')}$ in the above form is more restrictive than being free parameters: To simplify notation, let $C = C' = C''$, then $\boldsymbol{\alpha}^{i,j}_{(\lambda,\lambda')}$ has $C^2 K_u K_t$ many variables if all free. In comparison, $m^i_{(\lambda'',\lambda')}$ has $K_u C^2$ many variables, and $n^j_{(\lambda,\lambda'')}$ has $K_t C^2$ many, thus the rank-1 decomposed convolution formulation has only $(K_u + K_t)C^2$ many free variables in total. This quantifies the loss of expressiveness from (2) to (3).

B Details about Translate-Rotate MNIST Reconstruction

Here we provide the details of the translate-rotate mnist reconstruction experiments.

layer	Rank-1 3D	STDCF
conv1	$1 \times 3^2, 4, s(1,2,2)$ $3 \times 1^2, 4, s(2,1,1)$	$3 \times 3^2, 4, s(2,2,2)$ $(M = 5, N = 3)$
conv2	$1 \times 3^2, 8, s(1,2,2)$ $3 \times 1^2, 8, s(2,1,1)$	$3 \times 3^2, 8, s(2,2,2)$ $(M = 5, N = 3)$
deconv1	$1 \times 3^2, 4, s(1,2,2)$ $3 \times 1^2, 4, s(2,1,1)$	$3 \times 3^2, 4, s(2,2,2)$ $(M = 5, N = 3)$
deconv2	$1 \times 3^2, 4, s(1,2,2)$ $3 \times 1^2, 4, s(2,1,1)$	$3 \times 3^2, 4, s(2,2,2)$ $(M = 5, N = 3)$
conv3	$1 \times 3^2, 4, s(1,1,1)$ $3 \times 1^2, 1, s(1,1,1)$	$3 \times 3^2, 1, s(1,1,1)$ $(M = 5, N = 3)$

Table A: Architectures for Translate-Rotate MNIST reconstruction experiments. s(2, 2, 2) indicates the stride for 3D convolution.

Dataset. For training set, we randomly select 20,000 digits from original MNIST training set, and create 10,000 8-frame clips with 2 digits in each. For each clip, two digits start translation in random speeds from random positions, where the a digit will bounce backwards when it hit the border of the frame. The frame size is set to be 28, and the digit is formatted as the original MNIST 28×28 image. While the digit is translating, it is also rotating in a angular speed of 45 degree/frame to form complex spatiotemporal correlations. In additional, two digits can also overlap to make the reconstruction task more difficult. We construct 5,000 8-frame test clips in the same way of building the training set.

AutoEncoder Architecture and Training Details. We adopt a 2-layer 3D CNN for the encoder and 3-layer 3D CNN for the decoder. The autoencoder is instantiated by inserting the rank-1 decomposition or STDCF, as shown in Table A. For Training, we adopt the $L2$ loss, and use Adam optimizer with lr $= 1e-3$, batchsize 64. We train the model for total 50 epochs.

Additional Qualitative Results. We provide additional visualization results to show STDCF captures more spatiotemporal correlations than rank-1 decomposition. As shown in Figure A, STDCF consistently outperforms rank-1 decomposed 3D filters in reconstruction qualities.

C Details about the KTH experiments

We provide the architecture we used for KTH in both Section 2.1.2 and Section 3.1 in Table B. The 64-dimension representations shown in Figure 3 are obtained after conv3. the baseline method is the representation with $\tau_{test} = \tau_{train} = 1$. the tempo-awared methods is to use dilation=$(2, 1, 1)$ in all three convolutional layers. We provide more representation samples in Figure B.

Table B: Architectures for KTH experiment

layer	Reg. 3D	Rank-1 3D	STDCF
conv1	$5 \times 3^2, 16$	$1 \times 3^2, 16$ $5 \times 1^2, 16$	$5 \times 3^2, 16$ $(M = 5, N = 3)$
	max-pool $1, 2, 2$		
conv2	$5 \times 3^2, 32$	$1 \times 3^2, 32$ $5 \times 1^2, 32$	$5 \times 3^2, 32$ $(M = 5, N = 3)$
	max-pool $2, 2, 2$		
conv3	$3 \times 3^2, 64$	$1 \times 3^2, 64$ $3 \times 1^2, 64$	$3 \times 3^2, 64$ $(M = 5, N = 2)$
	max-pool $2, 2, 2$		
	global average pool, fc		

D Details about the Kinetics and Something-Somethingv1 experiments

D.1 Architecture

We provide the architecture of STDCF-R50 in Table C.

Table C: Architecture of STDCF-R50.

Stage	Layer	Output Size
raw	-	$L \times 224 \times 224$
conv_1	$5 \times 7 \times 7, 64$, stride 1, 2, 2	$L \times 112 \times 112$
pool_1	$1 \times 3 \times 3$, max, stride 1, 2, 2	$L \times 56 \times 56$
res_2	$\begin{bmatrix} 1 \times 1 \times 1, 64 \\ \text{STDCF } 3 \times 3 \times 3, 64 \\ 1 \times 1 \times 1, 256 \end{bmatrix} \times 3$	$L \times 56 \times 56$
res_3	$\begin{bmatrix} 1 \times 1 \times 1, 128 \\ \text{STDCF } 3 \times 3 \times 3, 128 \\ 1 \times 1 \times 1, 512 \end{bmatrix} \times 4$	$L \times 28 \times 28$
res_4	$\begin{bmatrix} 1 \times 1 \times 1, 256 \\ \text{STDCF } 3 \times 3 \times 3, 256 \\ 1 \times 1 \times 1, 1024 \end{bmatrix} \times 6$	$L \times 14 \times 14$
res_5	$\begin{bmatrix} 1 \times 1 \times 1, 512 \\ \text{STDCF } 3 \times 3 \times 3, 512 \\ 1 \times 1 \times 1, 2048 \end{bmatrix} \times 3$	$L \times 7 \times 7$
global average pool,fc		$1 \times 1 \times 1$

D.2 Accuracies of all ITSL iterations on Kinetics

We provided accuracies of all models learned in *stage-t* and *stage-s* of all three iterations on Kinetics-400 in Table D.

Table D: Accuracies of *stage-t* and *stage-s* models of all three iterations.

Method	Top-1 Acc.	Top-5 Acc.
STDCF-R50-t-1	68.2	88.4
STDCF-R50-s-1	70.8	89.1
STDCF-R50-t-2	72.0	89.7
STDCF-R50-s-2	73.1	90.2
STDCF-R50-t-3	73.6	90.3
STDCF-R50-s-3	74.0	90.6
STDCF-R50	74.5	91.2

D.3 Accuracies of all ITSL iterations on Something-Somethingv1

We provided accuracies of all models learned in *stage-t* and *stage-s* of all three iterations on Something-Somethingv1 in Table E.

Table E: Accuracies of *stage-t* and *stage-s* models of two iterations.

Method	Top-1 Acc.	Top-5 Acc.
STDCF-R50-t-1	42.3	71.8
STDCF-R50-s-1	44.1	73.6
STDCF-R50-t-2	44.8	74.3
STDCF-R50-s-2	45.1	74.7
STDCF-R50	45.9	75.2

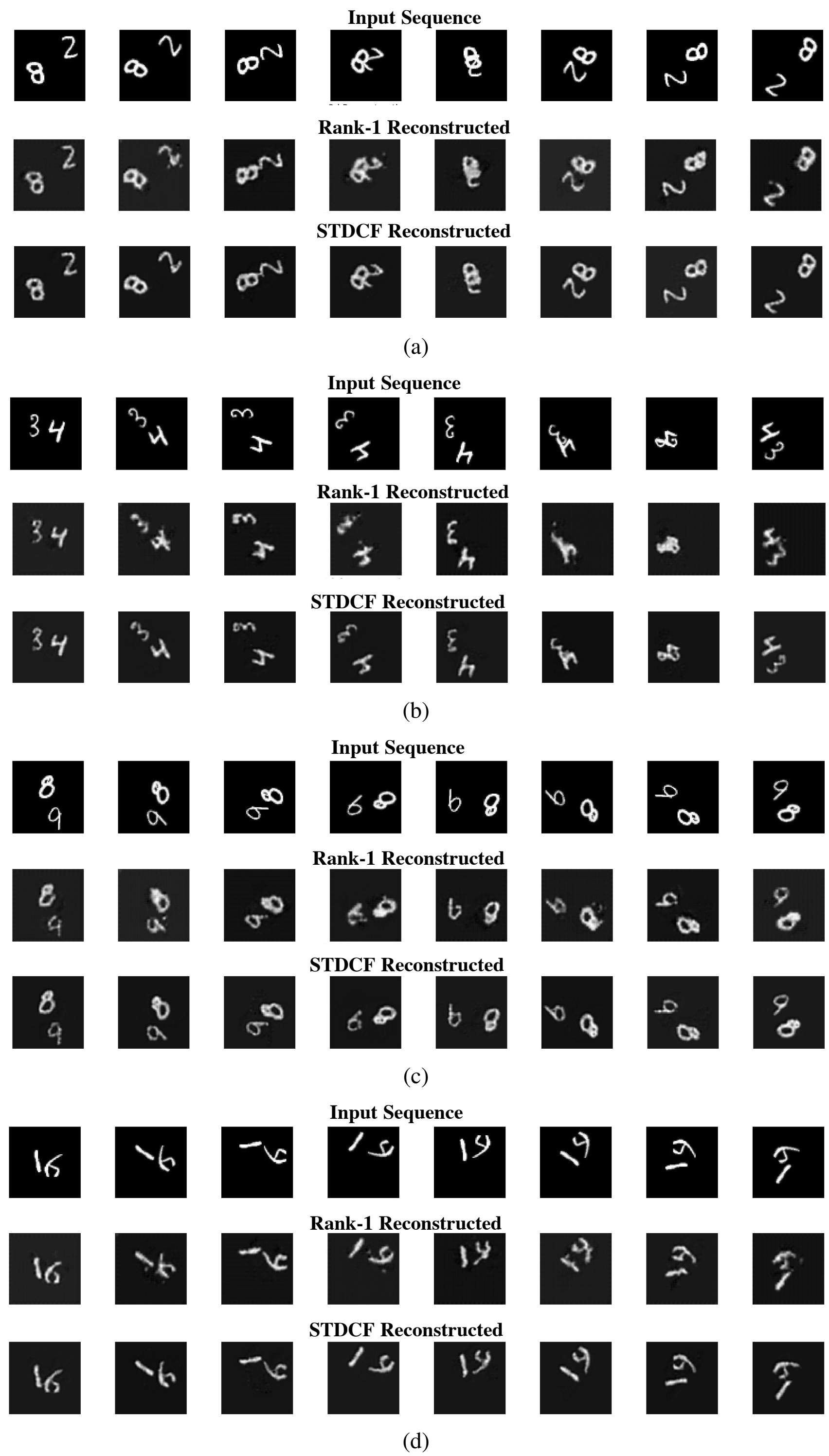

Figure A: More visualizations for TR-MNIST reconstruction.

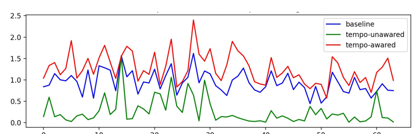

(a)

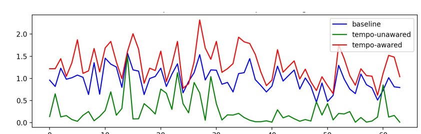

(b)

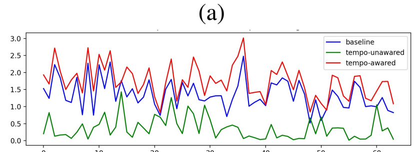

(c)

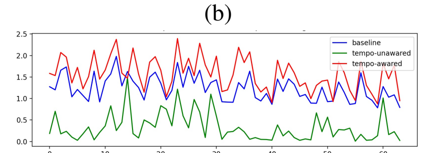

(d)

Figure B: More visualizations of representation comparisons.